DETERMINATION OF RADIATION FIELDS IN LIGHT WATER REACTOR INTERNALS USING PENTRAN™

Vefa N. Kucukboyaci[1] and Alireza Haghighat [2]
[1] Westinghouse Electric Co.
Science and Technology Department
1344 Beulah Road, Pittsburgh, PA 15246
kucukbvn@westinghouse.com

[2] University of Florida
Nuclear and Radiological Engineering Department
202 Nuclear Science Building, Gainesville, FL, 32611
haghighat@ufl.edu

ABSTRACT

We have performed discrete ordinates calculations to determine detailed three-dimensional neutron and gamma flux distributions in BWR reactor internals. Two-dimensional *(r-z)* adjoint function calculations have provided the relative contribution of different regions to the dpa per second (dpa/s) reaction at different reactor internals. Utilizing the adjoint data, we have inferred the effective 3-D model volumes/sizes for regions of interest; including core lower plate, jet pump assemblies, and core spray piping. Three-dimensional, multigroup (47-group neutron, 20-group gamma) flux maps have been calculated using the PENTRAN 3-D parallel S_N code in a relatively short amount of wall-clock time and with high parallel efficiency.

1. INTRODUCTION

Many components inside light water reactor vessels are made of stainless steel and various alloys are susceptible to displacement per atom (dpa) reaction and stress corrosion cracking (SCC). These materials degrade (in the forms of cracks) as the nuclear reactor ages. The amount of material degradation is expected to increase as the reactors approach their end of lifetimes. Further, this degradation can be accelerated by stresses from high temperature and pressure changes, chemical interactions, corrosive environments and radiation damage.

The degradation involves various reactor internals (control rod guide tubes, core shroud, shroud baffle plate, jet pump assemblies, core plates, top guide, feedwater spargers, and stand pipes), which have a critical role in the safe and continuous operation of a reactor. Therefore, it is necessary to accurately predict the fluence at these reactor components in order to justify the feasibility of a lifetime extension.

Accurate prediction of neutron and gamma fields in reactor internals requires performing three-dimensional, energy-dependent transport theory calculations. This requirement is due to following major reasons: geometric complexity, material heterogeneity, directional dependency of the source, significant flux attenuation, significant anisotropic scattering, and secondary gamma generation. A full detailed discrete ordinates (S_N) model can be prohibitive as it requires 100's of gigabytes of computer memory and large computation times. Hence, we take the following steps: i) Partition the

full model into overlapping models; ii) Determine the size of each model by performing 2-D adjoint ('importance') transport calculations; iii) Use PENTRAN [1], a 3-D parallel S_N code, to be able to handle the large memory and reduce the computation time.

In the past, we performed several simulations and analyses for determining the radiation field in a BWR core shroud [2, 3, 4]. In this study, we extend our previous studies to determine detailed three-dimensional neutron and gamma flux distributions inside a typical boiling water reactor vessel. In Section 2, we give a short overview of the adjoint function methodology and a brief description of the PENTRAN code system. Two-dimensional adjoint and 3-D forward calculations and their results are discussed in Section 3. Summary and conclusions are given in Section 4.

2. METHODOLOGY

2.1 ADJOINT FUNCTION METHODOLOGY

The reaction rate formulation in terms of adjoint function is given by [5]

$$R = < \Psi^{+} S > \tag{1}$$

where R is detector response, Ψ^{+} is adjoint (importance) function, and S is source. The Dirac signs ($< >$) refer to integration over phase space (i.e., space, energy, and angle). Here, we use this formulation to determine the contribution of different regions and energy groups to the dpa per second (dpa/s) at the important reactor internals. For example, regional contribution of gamma rays generated by (n,γ) interaction in a 2-D, spatially and energy-wise discretized S_N model can be determined by

$$Cij = \frac{S_{ij}^{*}}{\sum_{g} \phi_{ij,g}^{+n} S_{ij,g}^{n} + S_{ij}^{*}} \tag{2}$$

(I rewrote the formuation, is this ok?)

where, the adjoint weighted (n,γ) source is given by

$$S_{ij}^{*} = \sum_{g'} \phi_{ij,g'}^{+\gamma} \sum_{g} \sigma_{ij,g \to g'}^{(n,\gamma)} \phi_{ij,g}^{n} \tag{3}$$

Here, C is contribution, $\sigma^{(n,\gamma)}$ is the gamma-production cross-section for neutrons absorbed in energy group g and producing gamma rays into gamma energy group g', S is forward source, ϕ is forward scalar flux, ϕ^{+} is scalar adjoint function, i and j are spatial mesh indices, respectively. With this formulation, we calculate the fractional contribution of gamma rays generated by (n, γ) reaction to the dpa/s. Based on the fractional contributions, we can decide which regions to exclude from the whole 3-D model, and therefore infer the effective model size.

2.2 PARALLEL PROCESSING USING PENTRAN

PENTRAN (Parallel Environment Neutral-particle TRANsport) is a three-dimensional parallel discrete ordinates code designed for solving large and complex radiation transport problems in distributed-memory and distributed-computing environments. With its complete phase space domain decomposition formulations, memory partitioning, parallel I/O, adaptive differencing strategy,

variable meshing, and different iterative and acceleration techniques, PENTRAN yields accurate flux distributions in large/complex transport theory problems in short times. Thus far, PENTRAN has been used successfully for simulation of several real-life problems including: the VENUS-3 experimental facility [6], a BWR core shroud problem [2], the PGNAA (pulsed gamma neutron activation analysis) device [7] and an x-ray room [8]. These studies have demonstrated that PENTRAN yields accurate solutions, while maintaining a high parallel performance.

3. RESULTS AND DISCUSSION

3.1 TWO-DIMENSIONAL ADJOINT FUNCTION CALCULATIONS

The main purpose of the 2-D adjoint function calculations is to determine the regions that have the highest importance for the total dpa/s. By considering only these regions and eliminating the ones that have negligible contribution, we effectively reduce the size of the computation model, therefore reducing the computer memory and time. Three regions of interest (ROI) are considered for the adjoint simulations: core lower plate, jet-pump assembly, and core spray piping. We have developed separate DORT [9] *r-z* models with overlapping regions for each ROI. Dpa/s cross sections (47-group neutron, 20-group gamma) are placed in the ROI as the adjoint source. Adjoint ordered cross-sections are generated using the BUGLE-96 library [10]. A level-symmetric S_8 angular quadrature set and P_3 anisotropic scattering expansion are considered for these calculations.

Figure 1 shows the material distribution in Model 1 which includes the core lower plate as the ROI. In this model, the adjoint source (dpa/s cross-sections) is uniformly distributed throughout the lower plate region. Figure 2 shows both Model 2 and 3, with overlapping core, water gap, core shroud, jet pump, and pressure vessel regions. Note that these regions are also common in Model 1. The adjoint source is placed in a localized section in the jet pump region in Model2, whereas it is placed in the core spray piping region in Model 3. Table I summarizes the radial and axial dimensions and the regions included in the 2-D adjoint models.

Table I. Radial and Axial dimensions and regions covered in the 2-D adjoint models

Model	Radial Dimension (cm)	Axial Dimension (cm)	Regions
1 (Core Plate)	0.0-335.0	-432.59 – 190.5	Control Rod Drive Tubes, Core Support, Core Lower Plate, Core, Core Shroud, Jet Pump, Pressure Vessel
2 (Jet Pump)	0.0-335.0	-190.5 – 230.36	Core, Top Guide Grid, Core Shroud, Jet Pump, Pressure Vessel
3 (Core Spray)	0.0-335.0	-190.5 – 530.0	Core, Top Guide Grid, Shroud Head, Core Spray Pipes, Steam Separator Stand Pipes, Core Shroud, Jet Pump, Pressure Vessel

Figures 3a-b show the energy integrated contribution of neutrons and gamma rays, respectively, in Model 1. These figures indicate that neutrons and gamma rays in the vicinity of the core lower plate make the largest contribution to the dpa/s, and the importance decreases exponentially farther from the ROI. Comparing figures 3a and 3b shows that gamma rays are more directional and widely spread compared to neutrons. This is due to generation of secondary gamma rays through the (n,γ) process in the structural material and water. Similar behavior is observed in figures 4a-b and 5a-b for the jet pump and core spray piping models, respectively.

Table II shows the percent contribution of different regions to the dpa/s in core lower plate, jet pumps, and core spray pipes. In model 1, the major contributors to the dpa/s in the lower plate are the core

and the lower plate itself. In model 2, the major contributors to dpa/s in the jet pumps are the core and surrounding water body. In model 3, the major contributors to the dpa/s in the core spray pipes are the stainless-steel top guide and particle streaming through the steam region. Note that the 'X' mark in the table indicates that the corresponding region does not exist in that model.

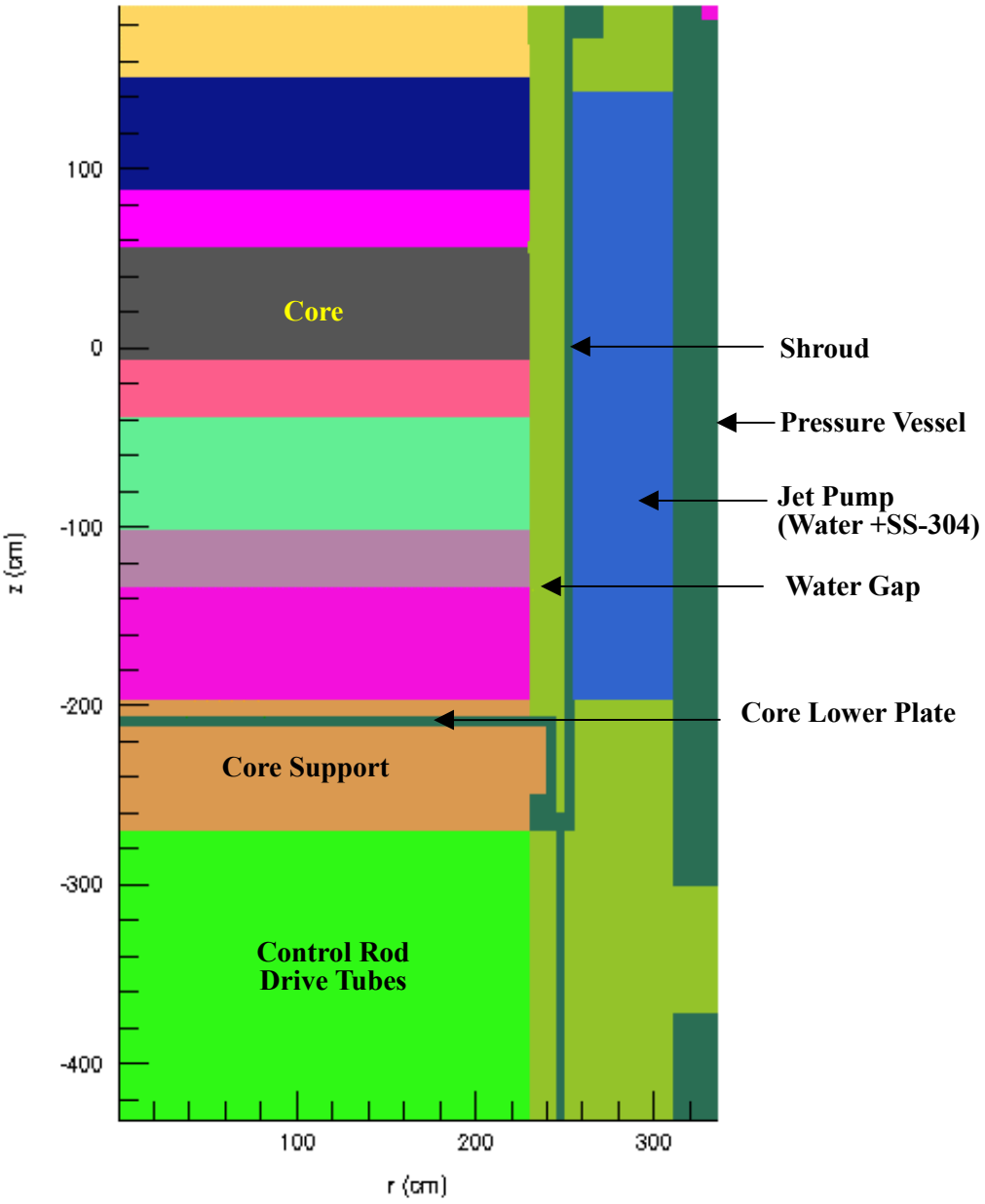

Figure 1. Model 1- Core lower plate 2-D *(r-z)* adjoint model

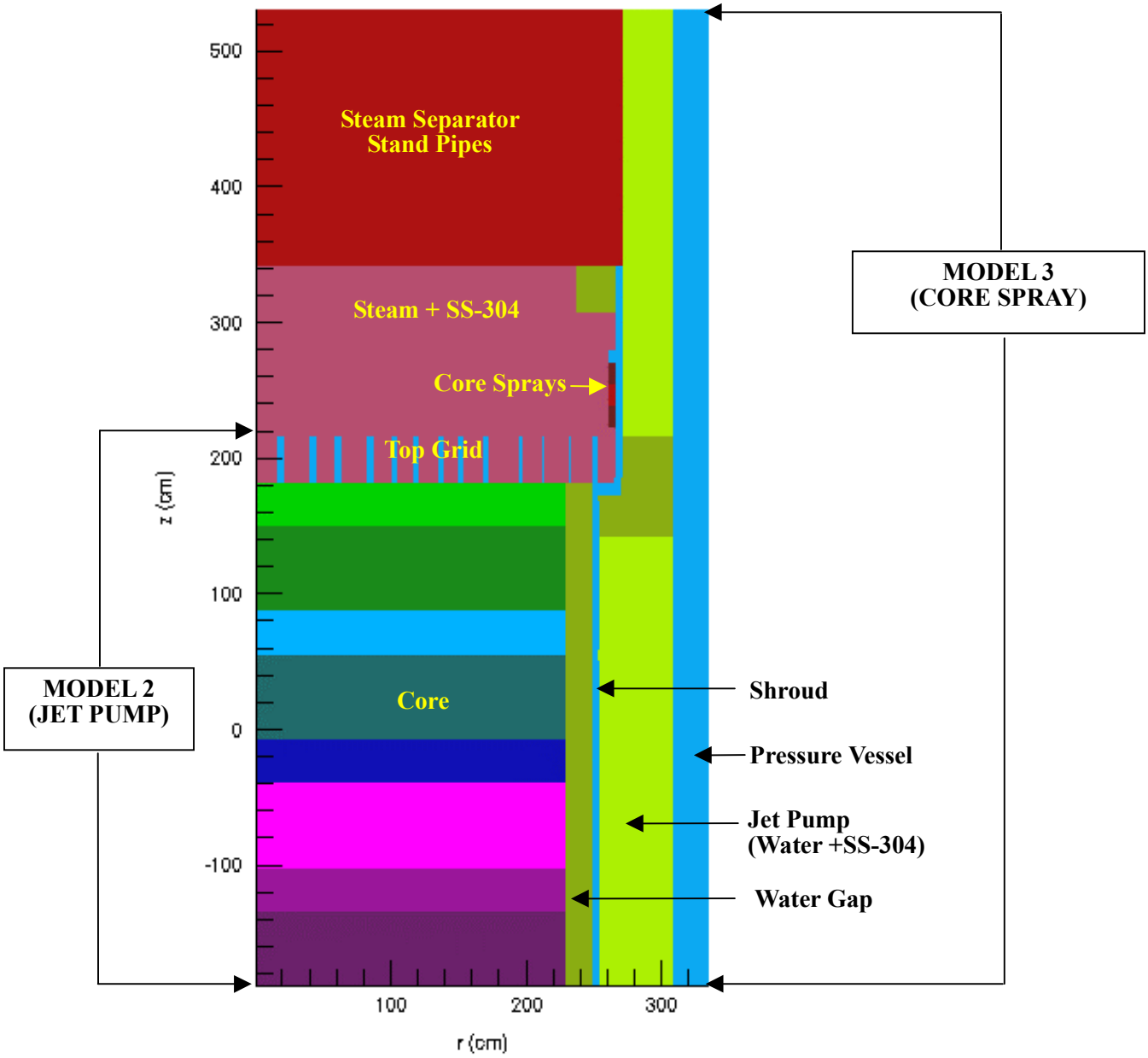

Figure 2. Models 1 and 2- Jet-pump and core spray pipes 2-D *(r-z)* adjoint models

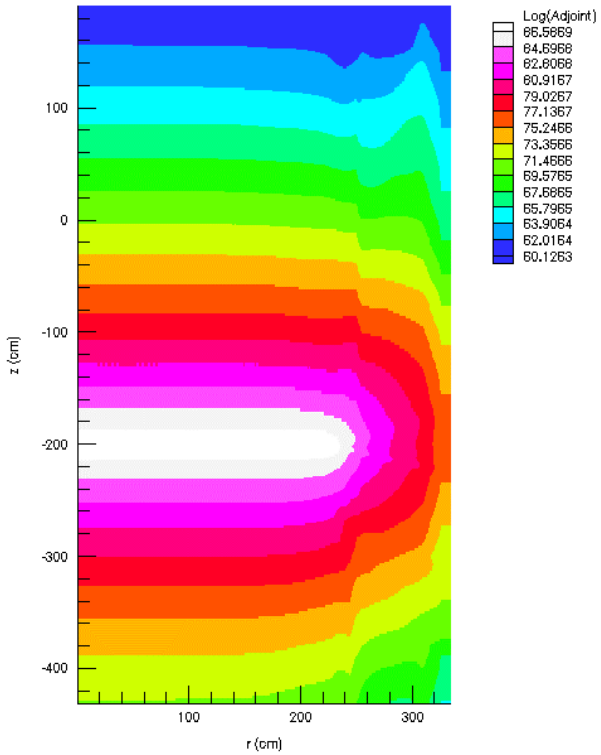

Figure 3a. Energy integrated contribution of neutrons to the dpa/s at the core lower plate.

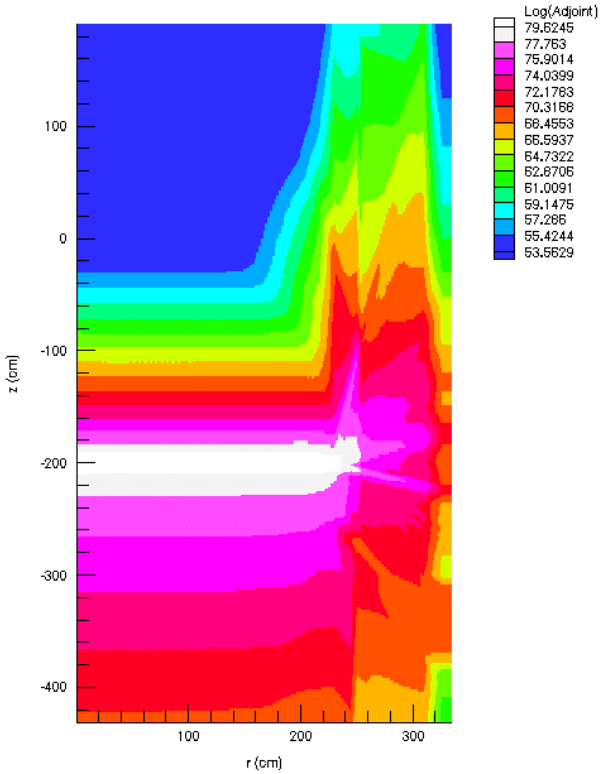

Figure 3b. Energy integrated contribution of gamma rays to the dpa/s at the core lower plate.

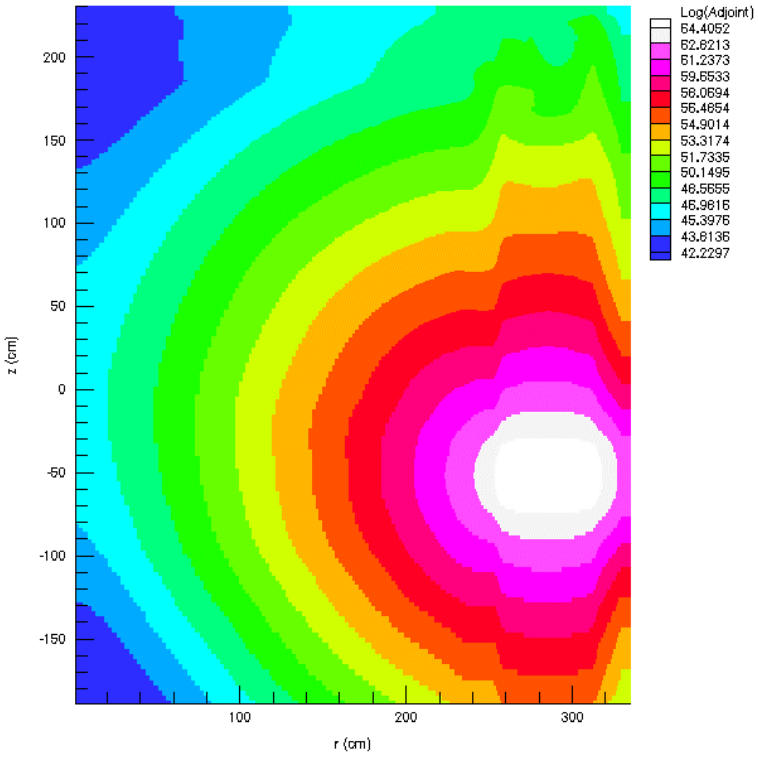

Figure 4a. Energy integrated contribution of neutrons to the dpa/s at the jet pump assembly.

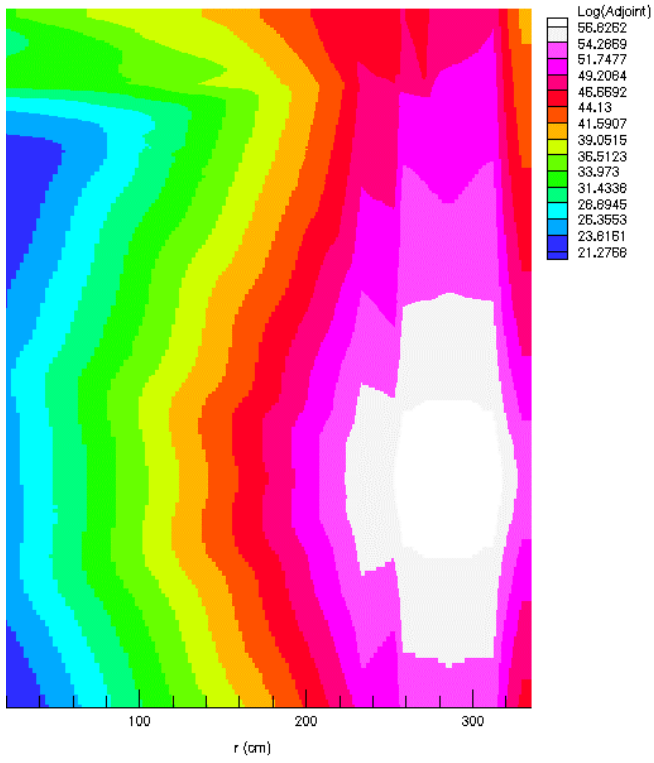

Figure 4b. Energy integrated contribution of gamma rays to the dpa/s at the jet pump assembly.

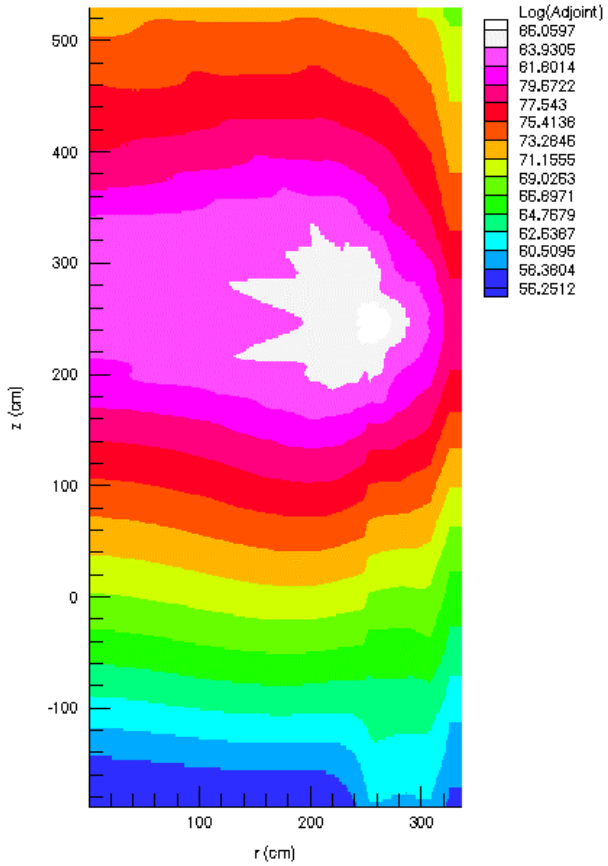

Figure 5a. Energy integrated contribution of neutrons to the dpa/s at the core spray.

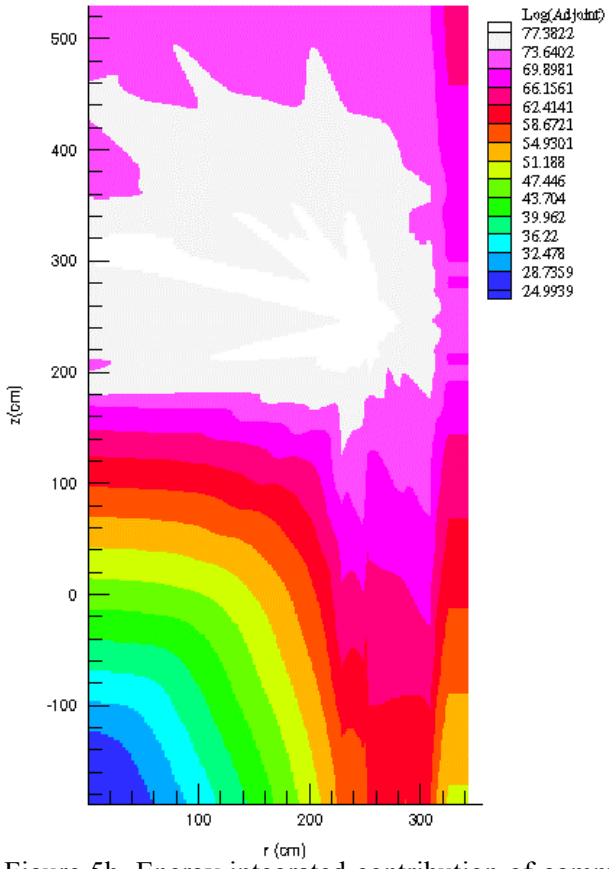

Figure 5b. Energy integrated contribution of gamma rays to the dpa/s at the core spray.

Table II. Percent contribution of different regions in the adjoint models

REGION	Contribution (%)		
	Model 1 (Core Lower Plate)	**Model 2 (Jet Pumps)**	**Model 3 (Core Spray Pipes)**
CRD Tubes	5.42E-06	X	X
Core Support	8.03E-01	X	X
Core Lower Plate	**3.92E+01**	X	X
Core	**5.95E+01**	**3.20E+01**	1.756E+01
Water Gap Between Core and Shroud	4.67E-01	**3.03E+01**	1.168E+00
Core Shroud	2.53E-09	1.91E+01	8.288E-01
Jet Pumps	8.17E-04	1.86E+01	9.669E-07
Pressure Vessel	1.88E-07	3.31E-02	3.479E-05
Top Guide	X	3.00E-05	**3.620E+01**
Steam Under Shroud Head	X	1.82E-06	**4.402E+01**
Steam Separator Stand Pipes	X	X	8.073E-02

3.2 THREE-DIMENSIONAL PENTRAN CALCULATIONS

Based on the importance function distribution and the regional contributions, we have partitioned the problem into three axially overlapping regions and inferred the effective sizes/volumes for the 3-D PENTRAN models.

Table III shows the axial and radial dimensions of the 3-D PENTRAN models. Model 1 with *221,760* fine meshes includes the Control Rod Drive tubes, core lower plate, and bottom part of the core. Model 2, with *332,640* fine meshes includes almost the full core height and the jet pump assemblies. Finally, Model 3, with *273,168* fine meshes includes upper fuel region, top grid assembly, and the core spray piping region. Note that core midplane is located at *z=0.0* cm. The effective radius of each model is *335* cm, which extends beyond the pressure vessel. Figures 6a-c show the 3-D mesh and material distributions of the three models.

Table III. Radial and axial dimensions 3-D PENTRAN models

Model	x-y Dimensions (cm)	Axial Dimension (cm)
1 (Core Plate)	0.0-300.0	-252.0 – -90.0
2 (Jet Pump)	0.0-300.0	-160.0 – 127.0
3 (Core Spray)	0.0-300.0	95.25 – 315.0

In PENTRAN, geometry is defined using coarse and fine meshes. Coarse meshes bound the subregions that can be processed in parallel. Inside each coarse mesh, there are fine meshes for which the actual transport sweeps are performed. Figure 7 represents the coarse and fine mesh distributions at different axial material regions prepared using PENMSH [11]. Note that each coarse mesh can have different number of fine meshes. For example, in the regions of interest, i.e., core lower plate, jet pump assemblies, and core spray piping; we have used small meshes in order to represent the curved boundaries and to preserve the volume, while we have used relatively large meshes away from these regions.

Quarter core symmetry is employed in all the models. An S_8 (80 directions in 3-D) symmetric angular quadrature and P_3 anisotropic scattering order are used in 3-D simulations. Void fraction dependent coupled neutron and gamma cross sections are generated using the BUGLE-96 library (47-group neutron, 20-group gamma). Source distribution is based on the Pennsylvania Power & Light Susquehanna BWR nuclear reactor unit 1 (SSES-1) assembly-wise power distribution and a reference source spectrum [12]. For higher solution accuracy, we have employed the adaptive differencing strategy of PENTRAN and accelerated the convergence of the source iterations using the Partial Current Rebalance acceleration. For parallel processing, we have partitioned the problem into 2 (Model 1) or 4 (Models 2-3) angular and 8 spatial subdomains and processed them on 16 or 32 processors. We have used the San Diego Supercomputer Center (SDSC) IBM-SP2 System with 332 MHz P2SC processors and 512 MB memory each. The memory requirement of each run is ~450 MB per processor.

We have computed the multigroup neutron and gamma fields in the three regions of interest. To illustrate the results, we present Figures 8a-c which show the neutron integral flux (> 0.1MeV), thermal neutron flux (E < 0.257 eV), and gamma flux (5.0 < E < 6.0 MeV) distributions in different models, respectively. We observe that flux levels of both neutrons and gamma rays are highest in the core region and they drop exponentially as the particles penetrate through several structural layers.

Previous analyses of the BWR core shroud calculations have shown that the gamma ray fluxes show fewer peaks and dips compared to neutron flux. This is due to generation of gamma rays in the water and the structural material. We observe similar behavior in the current results.

It is worth noting that since the three models have significant geometrical overlap, we observe that the solutions from different models in the overlap region agree with each other. Hence, we have effectively obtained the solution throughout the whole problem. Further, it is important to note that we could have solved the whole problem at once if we could have accessed more processors; the SDSC has 128 nodes with 8 processors per node, but requesting more processors and requiring more memory per processor would have caused prohibitive wait time in the queue.

The wall-clock times required for completing the 67-group, 3-D PENTRAN simulations for the three models are ~14 hr., ~12hr., and ~10 hr., respectively. These timing figures demonstrate that PENTRAN is quite efficient for rendering a very detailed solution in a minimum amount of wall-clock time and with a high parallel efficiency and scalability even for a large model.

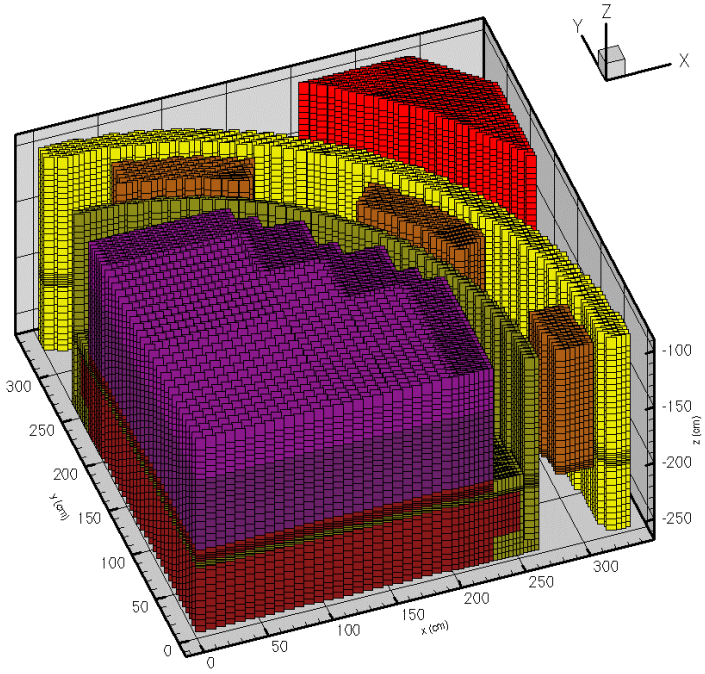

Figure 6a. Mesh and material distribution in 3-D PENTRAN model of the core lower plate region

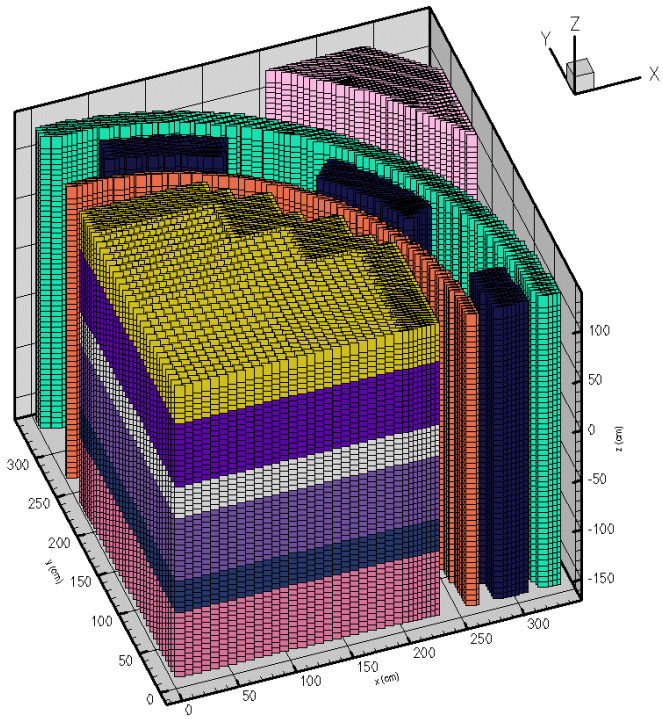

Figure 6b. Mesh and material distribution in 3-D PENTRAN model of the jet pump assembly region

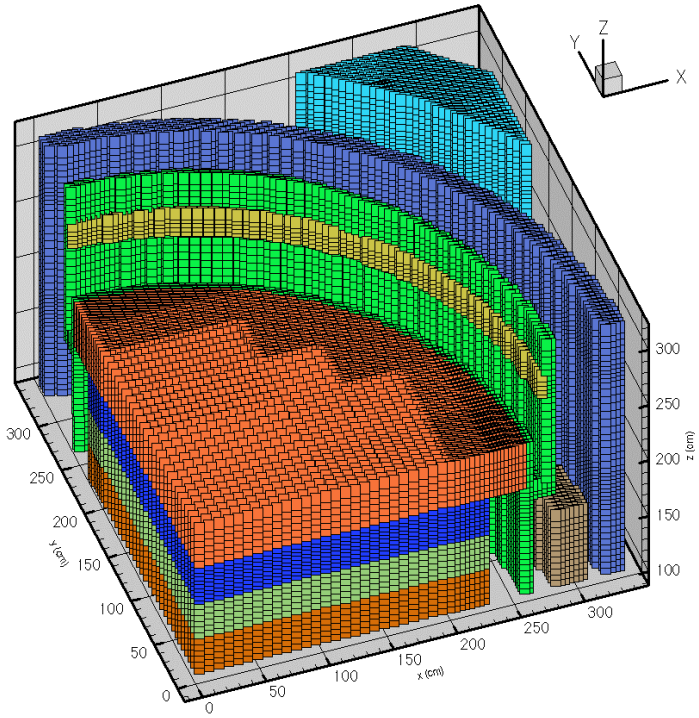

Figure 6c. Mesh and material distribution in 3-D PENTRAN model of the core spray piping region.

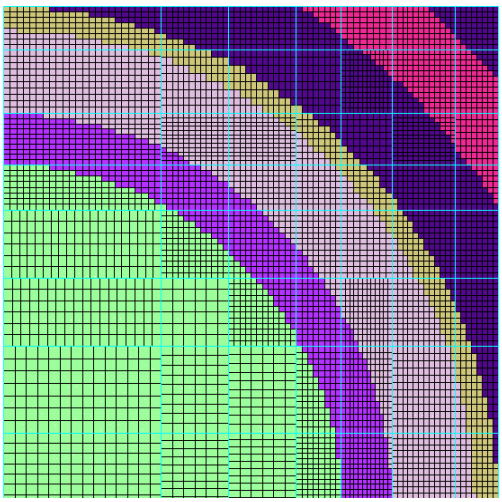

-252.0 cm < z < -241.8 cm

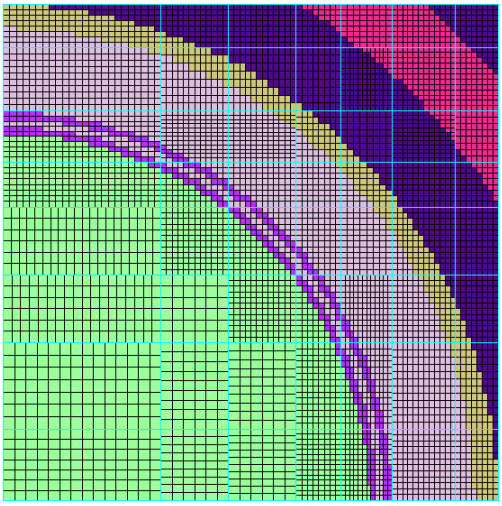

-231.68 cm < z < -193.0 cm

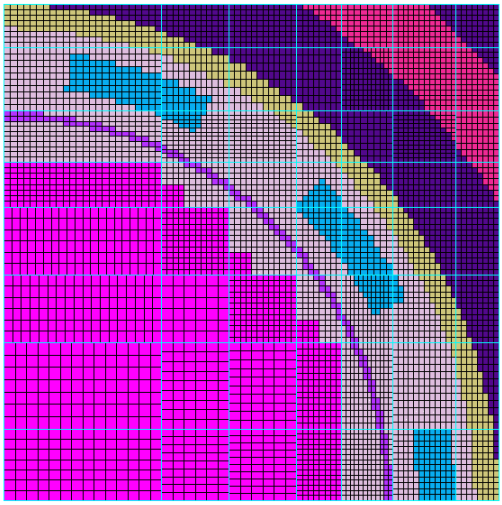

-188.0 cm < z < -160 cm

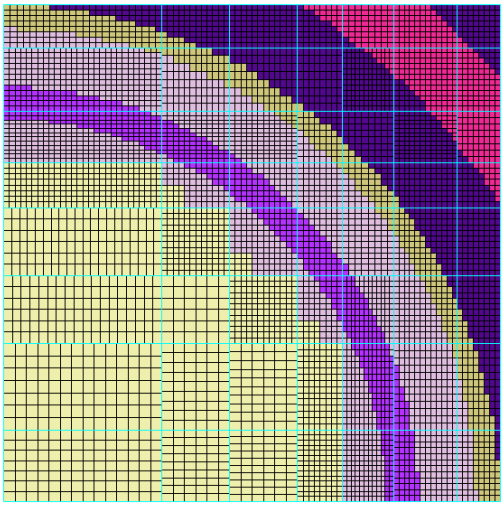

180.0 cm < z < 190.5 cm

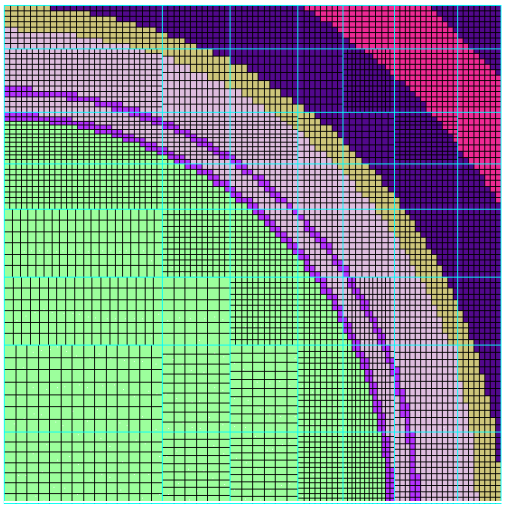

190.5 cm < z < 226.86 cm

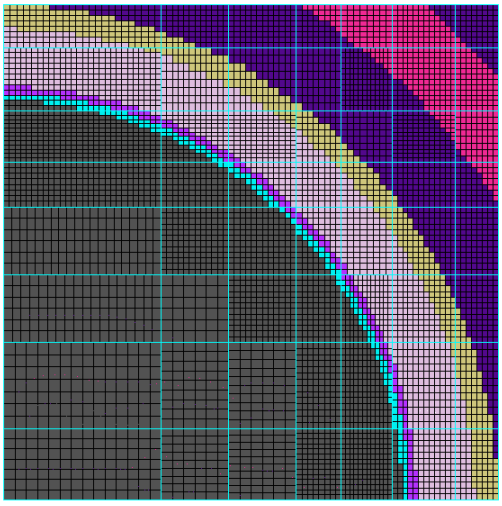

268.0 cm < z < 286.0 cm

Figure 7. Mesh and material distribution at various axial levels of the 3-D PENTRAN models

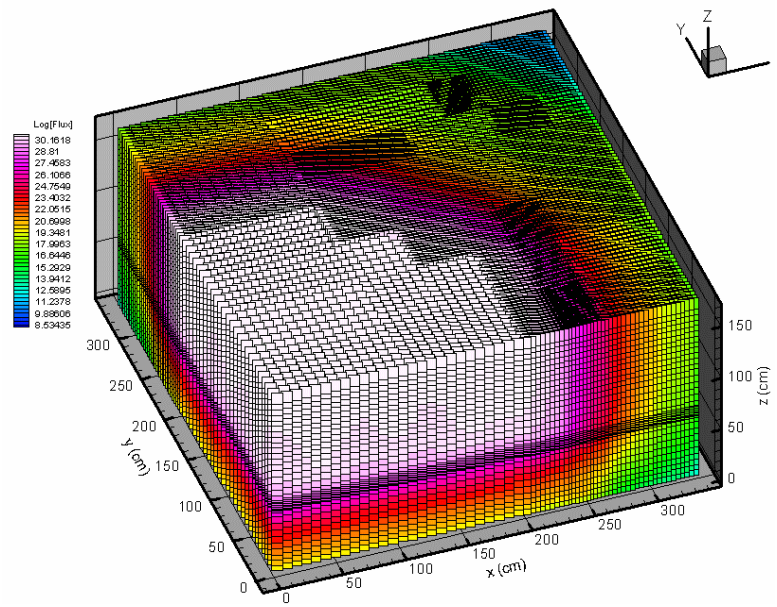

Figure 8a: Neutron integral flux (E>0.1 MeV) distribution in the core lower plate region (Model 1)

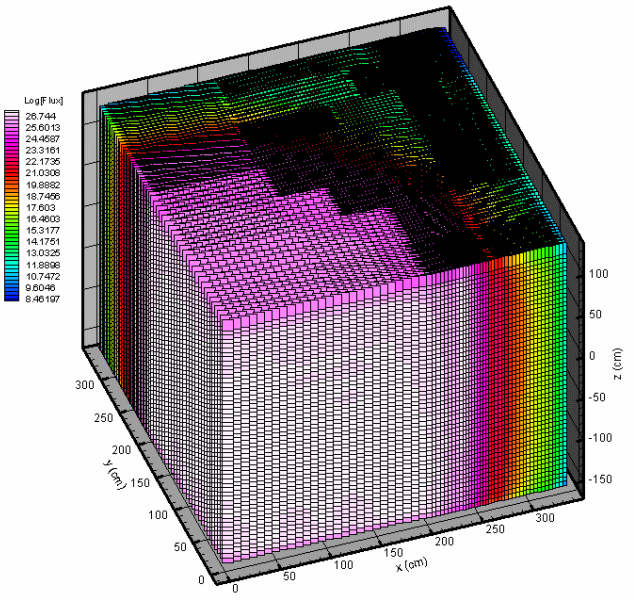

Figure 8b: Thermal neutron flux distribution (E < 0.257 eV) in Model 2.

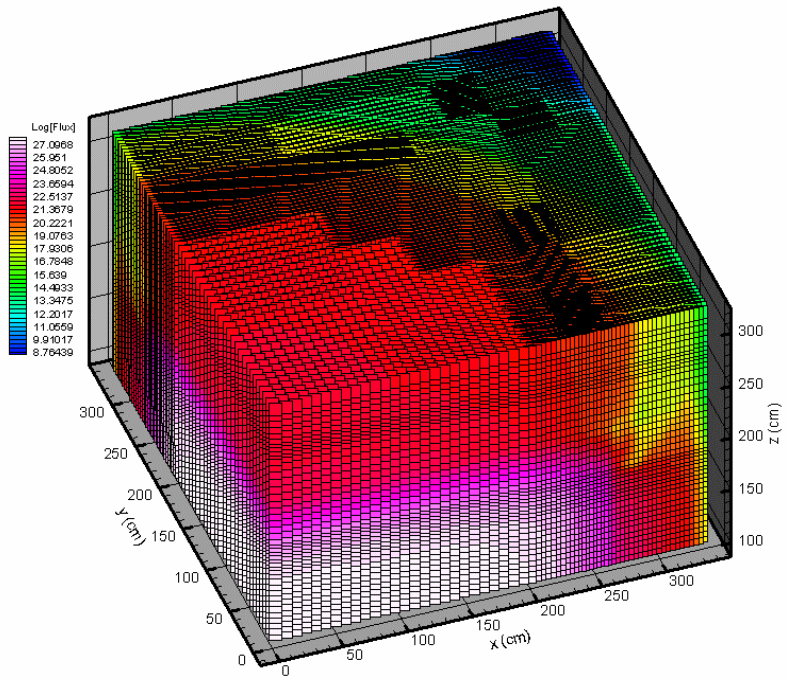

Figure 8c: Gamma flux (5.0 <E< 6.0 MeV) distribution in the core top-grid and spray piping region (Model 3)

CONCLUSIONS

We have performed discrete ordinates calculations to determine detailed three-dimensional neutron and gamma flux distributions in BWR reactor internals. Because of the large physical size, we have partitioned the model into three axially overlapping regions of interest, including: i) Core lower plate, ii) Jet-pump assemblies, and iii) Core spray piping. We have performed 2-D *(r-z)* adjoint function calculations to determine the regional contributions of neutrons and gamma rays to dpa/s and acquired effective model volumes/sizes for each region for subsequent 3-D models. Then, we have performed fixed source, 3-D Cartesian, 67-group (47-group neutron, 20-group gamma), P_3, S_8 discrete ordinates calculations using the PENTRAN code and obtained neutron and gamma fields in the reactor internals. These detailed neutron and gamma maps can further be used by the nuclear utilities to relate to the actual material damage through displacement per atom and/or to calculate the transmutation fraction of Boron and Nickel into Helium as a function of fluence.

REFERENCES

1. Sjoden G. and Haghighat A., "PENTRAN™: Parallel Environment Neutral-particle TRANsport in 3-D Cartesian Geometry", *Proc. Int. Conf. Mathematical Methods and Supercomputing for Nucl. Applications*, Saratoga Springs, NY, 1997
2. Kucukboyaci, V., A. Haghighat, G. Sjoden, and B. Petrovic, "Modeling of BWR or Neutron and Gamma Fields Using PENTRAN™," *Reactor Dosimetry*, ASTM STP 1398, John G. Williams, David W. Vehar, Frank H. Ruddy, and David M. Gilliam, Eds., ASTM, 2000.
3. B. Petrovic, A. Haghighat, A. Motta, V. Kucukboyaci and J. Kwon, "Impact of Gamma Irradiation on Material Damage in PWR Vessel and BWR Shroud," *Proc. 1998 Radiation Protection and Shielding Topical Conference*, Nashville, TN, April 20-23, 1998.
4. Haghighat, A., V. Kucukboyaci, G. Sjoden, and B. Petrovic, "Dose Estimation at a BWR Core Shroud Using PENTRAN," *Proc. Joint International Conference on Mathematical Methods and Supercomputing in Nuclear Applications*, Vol. I, 819-828, Saratoga Springs, NY, Oct. 6-10, 1997.
5. Bell, G. and S. Glasstone, *Nuclear Reactor Theory*, Malabar, Florida: Krieger, 1985.
6. A. Haghighat, H. A. Abderrahim, and G.E. Sjoden, "Accuracy and Parallel Performance of PENTRAN Using the VENUS-3 Benchmark Experiment", *Reactor Dosimetry*, ASTM STP 1398, John G. Williams, et al., Eds., ASTM, 2000.
7. B. Petrovic, A. Haghighat, T. Congedo, and A. Dulloo, "Hybrid Forward Monte Carlo-Adjoint Sn Methodology for Simulation of PGNAA Systems," *Proc. Int. Conf. M&C'99*, Madrid, Spain, pp. 1016-1025, Sept. 17- Oct. 1, 1999.
8. G.E. Sjoden, R. N. Gilchrist, D. L. Hall and C. A. Nusser, "Modeling a Radiographic X-Ray Imaging Facility with the PENTRAN Parallel SN Code," *Proc. of the PHYSOR 2000*, Pittsburgh, PA, May 7-11, 2000.
9. Rhoades, W. and R. Childs, "TORT/DORT: Two and Three – Dimensional Discrete Ordinates Transport", CCC-543, ORNL Radiation Shielding Information Center, Oak Ridge, TN (1991).
10. White, J.E. et al, "BUGLE-96: Coupled, 47 Neutron, 20 Gamma- Ray Group Cross Section Library," DLC-185, ORNL-RSIC, 1996.
11. A. Haghighat, "PENMSH - A 3-D Cartesian Mesh Generator for Sn Codes," Users Manual, Penn State Transport Theory Group, Penn State University, University Park, Dec., 1998, http://www.hsact.com.
12. A. Haghighat, M. Mahgerefteh, B. Petrovic, "Evaluation of Uncertainties in the Source Distribution for Pressure Vessel Neutron Fluence Calculations", *Nucl. Tech.*: 109, 54, 1995.